Second harmonic generation of a uniaxial antiferromagnetic film

Siew-Choo Lim
School of Physics, Universiti Sains Malaysia, 11800 Minden, Penang, Malaysia

(Received 16 September 2001)

The second harmonic generation (SHG) of a uniaxial antiferromagnetic film based on antiferromagnetic response is calculated and analyzed by using conventional nonlinear optics approach. Within this approach, the theoretical modeling assumed weak nonlinearity and no depletion of incident waves. In the studies, in order to observe second harmonic (SH) transmission and reflection through the film, the antiferromagnetic film is configured with reference to the non-vanishing linear and second harmonic susceptibility tensor elements of the antiferromagnetic system. With these, some of the second harmonic transmissions and reflections versus frequency and thickness are calculated numerically and shown graphically.

Keywords: Antiferromagnet; nonlinear; second harmonic generation

I. INTRODUCTION

The simplest nonlinear response in a physical system subjected to incident electromagnetic radiation is second harmonic generation (SHG) [1]. In the study of nonlinear effects in dielectrics, weak nonlinear approach is usually used [1,2]. This approach has been extended to the magnetic systems and it obviously open up a simpler way to study various nonlinear effects in magnetic systems [3-5]. By using the weak nonlinear assumption, the dynamic magnetization m can be expanded in power series of the incident dynamic magnetic fields h:

$$m_i = \chi_{ij} h_{ij} + \chi i_{ijk} h_j h_k + \chi_{ijkl} h_j h_k h_l + \ldots \qquad (1)$$

With this, the complete linear and nonlinear susceptibility tensors up to third order effects for a uniaxial antiferromagnet have been calculated and analyzed subjected to single frequency incident electromagnetic waves [5].

II. FORMALISM

The non-vanishing linear and second harmonic susceptibility tensor elements of an antiferromagnet are used to determine the suitable model for the observation of second harmonic effects. From our previous calculations, the independent non-vanishing linear and nonlinear elements up to second harmonic effects in Cartesian system, (xyz), are χ_{xx}, χ_{xy}, χ_{yx}, χ_{yy}, χ_{xxz}, χ_{xyz}, χ_{yxz}, χ_{yyz}, χ_{zxx} and χ_{zyy}. The full mathematical expressions of the elements are given in our previous paper [5].

Based on these non-vanishing elements, the practical model is the antiferromagnetic film in the configuration of Voigt geometry as shown in Fig.1.

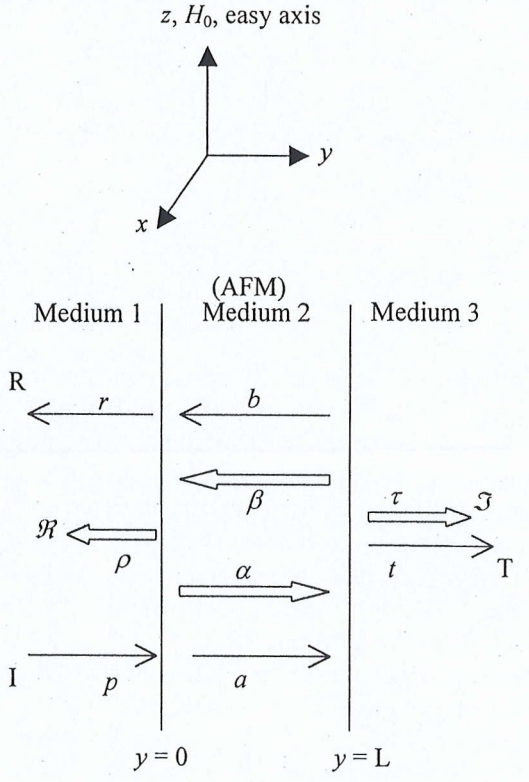

FIG. 1. Antiferromagnetic film in Voigt geometry.

Here we set y as the direction of incident waves, I, and the rf H fields in I are x-polarized. All these configurations will determine which elements should be taken into account due to the transverse nature of

electromagnetic waves. These are: χ_{xxx}, χ_{xyy}, χ_{yyx}, χ_{yyy}, χ_{zxx} and χ_{zyy}.

Based on these assumptions, the wave equations derived from the Maxwell's equations and the appropriate constitutive relations are

$$\frac{\partial^2 H_{xo}(y)}{\partial y^2} + k_y^2 H_{xo}(y) = 0 \qquad (2)$$

for linear waves and

$$\frac{\partial^2 H_{zo}(y)}{\partial y^2} + k_z^2 H_{zo}(y) = \Gamma H_{xo}(y) H_{xo}(y) \qquad (3)$$

for second harmonic waves. Here $H_{zo}(y)$ is the induced second harmonic rf H fields due to the existence of nonzero χ_{zxx} and χ_{zyy}. The other terms

$$k_y = \omega \sqrt{\varepsilon_o \mu_o \left(1 + \chi_{xx} + \frac{(\chi_{xy})^2}{1+\chi_{xx}}\right)}$$

and

$$k_z = \Omega \sqrt{\varepsilon}/c ; \Omega = 2\omega \qquad (4)$$

represent the magnitude of linear and SH propagation vector, and

$$\Gamma = -\frac{1}{2}\varepsilon\varepsilon_0\mu_0\Omega^2\chi_{xx}\left\{1+\left(\frac{\chi_{xy}}{1+\chi xx}\right)^2\right\} \qquad (5)$$

is a function of linear and SH susceptibility elements and is corresponding to the generation of SH waves. Eq. (2) is a homogeneous linear second order differential equation for $H_{x0}(y)$ and Eq. (3) is an inhomogeneous linear second order differential equation for $H_{z0}(y)$ with a source in terms of $H_{x0}(y)$. The results in Eqs. (2) and (3) are obtained by weak nonlinearity approach and without slowly varying envelope approximation (SVEA), and we also assume that there is no depletion of the input waves. Based on Eq. (2), the general solutions for the linear waves $H_x(y, t)$ and $E_z(y, t)$ are

$$H_x(y,t) = \frac{1}{2}\left[a\exp(ik_y y) + b\exp(-ik_y y)\right]\exp(-i\omega t) + c.c. \qquad (6)$$

and

$$E_z(y,t) = \frac{1}{2}\frac{k_y}{\varepsilon_0\varepsilon\omega}\left[a\exp(ik_y y) - b\exp(-ik_y y)\right]\exp(-i\omega t) + c.c. \qquad (7)$$

From Eq. (3), the general solutions for the second harmonic waves $H_z(y, t)$ and $E_x(y, t)$ are

$$H_z(y,t) = \tfrac{1}{2}\left[\alpha\exp(ik_z y) + \beta\exp(-ik_z y) + f_1\exp(i\xi y) + f_2\exp(-i\xi y) + f_3\right] \times\exp(-i\Omega t) + c.c. \qquad (8)$$

and

$$E_x(y,t) = \tfrac{1}{2}\frac{1}{\varepsilon_0\varepsilon\Omega}\left[-\alpha k_z\exp(ik_z y) + \beta k_z\exp(-ik_z y) - f_1\xi\exp(i\xi y) + f_2\xi\exp(-i\xi y)\right]\times\exp(-i\Omega t) + c.c. \qquad (9)$$

where

$$f_1 = \frac{\Gamma a^2}{(k_z^2 - \xi^2)}, f_2 = \frac{\Gamma b^2}{(k_z^2 - \xi^2)}, f_3 = \frac{2ab\Gamma}{k_z^2} \qquad (10)$$

for phase mismatch ($k_z \neq 2k_y \neq \xi$), and

$$H_z(y,t) = \frac{1}{2}\left[(\alpha + yd_1)\exp(i\xi y) + (\beta + yd_2)\exp(-i\xi y) + d_3\right] \times\exp(-i\Omega t) + c.c. \qquad (11)$$

$$E_x(y,t) = \frac{1}{2}\frac{1}{\varepsilon_0\varepsilon\Omega}\left[(-\alpha\xi + id_1 - \xi y d_1)\exp(i\xi y) + (\beta\xi + id_2 + \xi y d_2)\exp(-i\xi y)\right] \times\exp(-i\Omega t) + c.c. \qquad (12)$$

where

$$d_1 = \frac{\Gamma a^2}{i2\xi}, d_2 = \frac{\Gamma b^2}{-i2\xi}, d_3 = \frac{2ab\Gamma}{\xi^2} \qquad (13)$$

for phase matching $(k_z = 2k_y = \xi)$.

In the equations, ω and Ω are the incident and second harmonic frequency. a, b and α, β are the superposition coefficients for the homogeneous solutions of Eqs. (2) and (3). The linear amplitude coefficients a, b, r, t, and the second harmonic amplitude coefficients α, β, ρ, τ are determined by applying the antiferromagnetic film boundary conditions to the tangential H and E fields of the waves propagation as shown in the schematic diagram in Fig. 1, namely the conservation of these rf fields across the film boundaries. With the resulting linear coefficients r and t, and second harmonic coefficients ρ and τ, the calculations of Poynting's vector in each medium show that the transmission and reflection coefficients through the antiferromagnetic film are

$$T = \frac{\varepsilon_1}{\varepsilon_3}\frac{|t|^2}{|p|^2} \text{ and } R = \frac{|r|^2}{|p|^2} \text{ for linear waves,} \quad (14)$$

and

$$\mathfrak{I} = \frac{\varepsilon_1}{\varepsilon_3}\frac{|\tau|^2}{|p|^2} \text{ and } \mathfrak{R} = \frac{|\rho|^2}{|p|^2} \text{ for second harmonic waves,} \quad (15)$$

where ε_1 and ε_3 are the dielectric constants for medium 1 and medium 3 that sandwich the antiferromagnetic film. p is the coefficient for the amplitude of input waves, and $|p|^2$ is directly proportional to the input power I_p where $I_p = \frac{1}{2}\frac{k_1}{\varepsilon_0 \varepsilon \omega}|p|^2$.

III. RESULTS AND DISCUSSION

The transmission and reflection coefficients in Section 2, Eqs. (14) to (15) are shown graphically by using the parameters of FeF_2. For temperature equals to 15 K, these parameters are ε =5.5 for dielectric constant, γ/μ_0 = 1.05 $cm^{-1}Tesla^{-1}$ for gyromagnetic ratio, $\mu_0 H_E$ = 53.3 Tesla for exchange field, $\mu_0 H_A$ = 19.7 Tesla for anisotropy field, $\mu_0 M_0$ = 0.056 Tesla for sublattice magnetization [6] and $\mu_0 H_0$ for applied static field. In the calculations, the chosen damping parameter is $\eta = 5 \times 10^{-4}$ [5]. The linear and second harmonic transmission and reflection coefficients are plot versus frequency sweep with fixed thickness and applied static fields. These are shown in Figs. 2 and 3 for $\mu_0 H_0$ = 4 Tesla. In Figs. 4 and 5, we show the linear and SH transmission

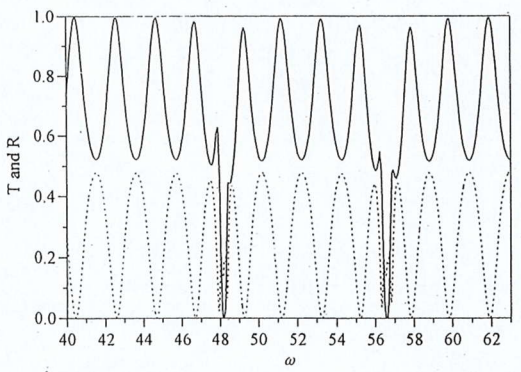

FIG. 2. Linear transmission T (___) and reflection R (----) versus input frequency (cm^{-1}) for a 1 mm antiferromagnetic film in 4 Tesla magnetic field.

and reflection coefficients versus thickness for $\mu_0 H_0$ = 3 Tesla and input frequency ω = 55 cm^{-1}. The input intensity to produce the results in Figs. 2 to 5 is $I_p = 1.6 \times 10^{15}$ Wm^{-2}. If the FIR is focused to a 0.5 mm^2 beam, the strength of H field is approximately 18 Gauss, and is achievable currently [3].

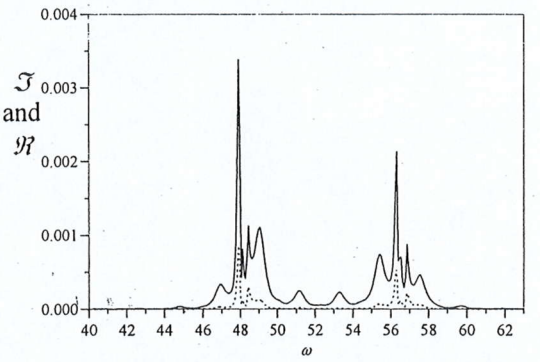

FIG.3. Second harmonic transmission $\mathfrak{I}$ (_____) and reflection $\mathfrak{R}$ (-------) versus input frequency (cm^{-1}) for a 1 mm antiferromagnetic film in 4 Tesla magnetic field.

From Fig. 2, the linear transmission and reflection show clearly that there are two antiferromagnetic resonances for x-polarized input waves in the present of static applied magnetic field $\mu_0 H_0$ as implied in the linear antiferromagnetic susceptibility. These resonances occurred at frequency $\omega_p = \omega_R - \omega_0$, and $\omega_n = \omega_R + \omega_0$, in which ω_R is the resonance frequency for antiferromagnet and $\omega_0 = \gamma H_0$ is the frequency shifts due to the applied static field $\mu_0 H_0$. For FeF_2, ω_R = 52.4 cm^{-1}, and for 3 Tesla applied static field, the gap between the p-resonance and n-resonance, $\omega_g = 2\omega_0$, will be 6.3 cm^{-1}. These are shown clearly in Figs. 2 and 3. The dips at the resonances for both transmission and reflection curves are due to the strong linear antiferromagnetic absorption at the resonance frequencies, whereas the peaks and troughs away from resonance are due to the dimensional resonance depending on the wave vector, k_v, and the thickness of the film, L.

The SH transmission and reflection, $\mathfrak{I}$ and $\mathfrak{R}$ are significant only in the vicinities of antiferromagnetic resonances. From the curves shown in Figs. 3 to 5, and the model shown schematically in Fig. 1, it is obvious that the peaks and troughs of $\mathfrak{I}$ and $\mathfrak{R}$ curves are due not only to the antiferromagnetic and dimensional resonance, but also affected by the input resonance (standing waves in the films that generating T) and output resonance (standing waves in the films that generating R) of the linear waves. With all these resonance enhancement, the signals shown in $\mathfrak{I}$ and $\mathfrak{R}$ would not be regular peaks and troughs as the linear transmission and reflection but somehow irregular especially in the vicinities of the antiferromagnetic resoannces. These are shown clearly in Figs. 3 and 5

when compare the existence of $\mathcal{T}$ and $\mathcal{R}$ peaks to the peaks of linear transmission.

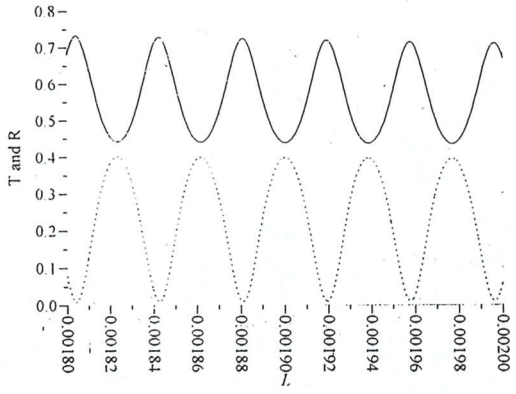

FIG. 4. Linear transmission T (____) and reflection R (-----) versus film thickness (meter) for an antiferromagnetic film in 3 Tesla magnetic field and input frequency $\omega = 55\ \text{cm}^{-1}$.

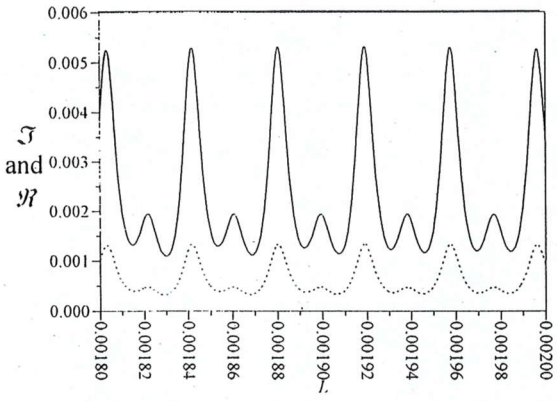

FIG. 5. Second harmonic transmission $\mathcal{T}$ (____) and reflection $\mathcal{R}$ (-------) versus film thickness (meter) for an antiferromagnetic film in 3 Tesla magnetic field and input frequency $\omega = 55\ \text{cm}^{-1}$

In conventional nonlinear optics, the second harmonic generation signal are significant when phase-matching occurred. However, from the approaches of this paper, it is obvious that with the complex linear and second harmonic susceptibilities, there is no chance to achieve phase-matching for the antiferromagnetic films. The peaks and troughs show in $\mathcal{T}$ and $\mathcal{R}$ can be described as the pseudo-phase-matching when one or more of the resonance enhancements described above occurred. The other important feature of the second harmonic transmission and reflection is that $\mathcal{T}$ and $\mathcal{R}$ has no phase difference if compared to the linear transmission and reflection with $\pi/2$ phase difference. The reason is the second harmonic output, $\mathcal{T}$ and $\mathcal{R}$ has no input from the medium in the left of the antiferromagnetic film as for the linear case. The only difference of $\mathcal{T}$ and $\mathcal{R}$ is in terms of magnitudes in which $\mathcal{T}$ is greater than $\mathcal{R}$ because of the input resonance that affected $\mathcal{T}$ directly is stronger than the output resonance.

IV. CONCLUSION

The main result of this paper is the calculation and formulation for the generation of SH waves through an antiferromagnetic film based entirely on the magnetic response of an antiferromagnet rather than the magneto-optical effects based on electrical response that affected by the existence of the magnetization [7]. The calculation here make use of the conventional approach, where for weak nonlinearity, less than 1 % of the input intensity are converted to SH waves, therefore the assumption of no depletion of the input waves is used to simplify the calculation. However, the approach we used here is slightly varying from the usual formulation in nonlinear optics in which we are neglecting the SVEA [8].

The approach we used here may open another possible way, i.e., conventional nonlinear optics approach, to study and characterized the nonlinear effects and their applications in magnetic systems. And it may be extend to more sophisticated cases such as the generation of SH waves with depletion of input waves in magnetic superlattices.

ACKNOWLEDGEMENT

This work was supported by the research grant provided by Universiti Sains Malaysia, Penang.

REFERENCES

[1] P.N. Butcher and D. Cotter, *The elements of nonlinear optics*, Cambridge University Press, Cambridge (1990).
[2] D.L. Mills, *Nonlinear optics*, 2nd Ed., Springer, New York (1998).
[3] N.S. Almeida and D.L. Mills, Phys. Rev. B, **36**, 2015 (1987).
[4] S.C. Lim, J. Osman and D.R. Tilley, J. Phys. D: Appl., **32**, 755 (1999).
[5] S.C. Lim, J. Osman and D.R. Tilley, J. Phys. D: Appl., **33**, 2899 (2000).
[6] K. Abraha and D.R. Tilley, Surface Science Reports, **24**, 125 (1996).
[7] V.N. Gridnev, Solid State Communications, **100**, 71 (1996).
[8] N. Hashizume, M. Ohashi, T. Kondo and R. Ito, J. Opt. Soc. Am. B, **12**, 1894 (1995).